

Supporting Information

***In-situ* SERS Study of Ionic Transport and Joule Heating Effect in Plasmonic Nanopores**

Jin-Mei Yang,^a Zhong-Qin Pan,^a Fei-Fei Qin,^b Ming Chen,^a Kang Wang,^{a*} and Xing-Hua Xia^a

^a State Key Laboratory of Analytical Chemistry for Life Science, School of Chemistry and Chemical Engineering, Nanjing University, Nanjing 210023, China

^b Department of Physics, Southeast University, Nanjing 210096, China

Table of contents

S1. Chemicals and reagents

S2. Instruments

S3. Synthesis of Au nanoparticles (AuNPs)

S4. Fabrication and modification of the SERS-active hydrophilic gold porous structure (*hydro-GPS*)

S5. The internal structure of the *hydro-GPS*

S6. Electrochemical and SERS spectroscopy measurements

S7. SERS activity and electrochemical properties of the *hydro-GPS*

S8. FDTD simulation

S9. Control experiments

EXPERIMENTAL SECTION

S1. Chemicals and Reagents

HAuCl₄·4H₂O, 3, 6-dioxa-1, 8-octanedithiol (DODT), 4-methoxyphenyl isocyanide (MOPI), and tetraoctylammonium bromide (TOAB) are purchased from Sigma-Aldrich. All chemicals are analytical grade. All aqueous solutions are prepared with Millipore water (resistivity ≥ 18.2 M Ω ·cm).

S2. Instruments

Morphologies of materials are characterized by scanning electron microscopy (SEM, S-4800, Japan) and transmission electron microscopy (TEM, JEM-2100, Japan), respectively. UV-vis absorption spectra are recorded on Nanodrop-2000C spectrophotometer (Thermo Fisher Scientific, Inc.). A FEI Helios 600i focused ion beam (FIB, Czech Republic) is used to analyze the internal structure of *hydro*-GPS. The zeta potential measurements are performed with a Malvern Zetasizer Nano ZS90 analyzer at room temperature. The glass nanopipettes are pulled on a CO₂-laser-based pipette puller (P-2000, USA) with glass capillaries (O.D. 1.0 mm and I.D. 0.58 mm, Sutter, BF100-58-10). The bias potential applied on the electrochemical cell is powered by an electrochemical working station (CHI 660E, China).

S3. Synthesis of Au nanoparticles (AuNPs)

Gold nanosphere seeds are synthesized by using the citrate-reduction method reported by Frens¹. Briefly, 2 mL of 1% trisodium citrate is added to 50 mL of 0.01% HAuCl₄ refluxing solution under vigorous stirring, and the mixture is kept boiling for another 15 min. The solution color turns to wine red, indicating the formation of AuNPs (~2.21 nM). Then, the solution is cooled down to room temperature with continuous stirring. The prepared colloid AuNPs are stored in brown glass bottles at 4 °C. The diameter of the synthesized AuNPs is 15±1.5 nm and the maximum extinction wavelength is 519 nm (Figure S1).

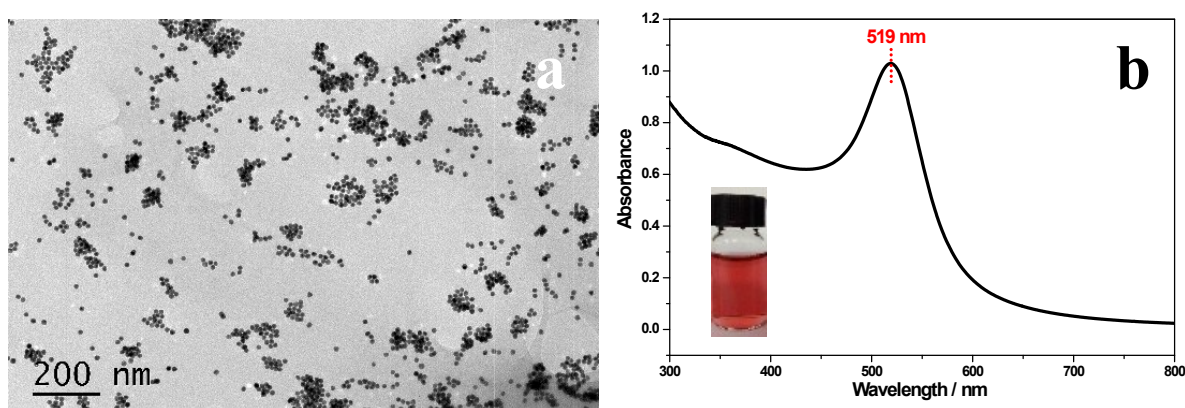


Figure S1. TEM (a) and UV-Vis absorption spectrum (b) of the 15 nm AuNPs.

S4. Fabrication and modification of the SERS-active hydrophilic gold porous structure (*hydro*-GPS)

The procedure of hydrophilic gold porous structure (*hydro*-GPS) manufacturing is outlined schematically in Figure 1a. Firstly, the glass capillaries are pulled into glass nanopipettes with tip orifice of ~ 100 nm (Figure S2a). Then, the nanopipettes are filled with ~ 10 μ L aqueous solution of DODT (7.5 mM) and kept in air for about 0.5 h to infiltrate the very end of the tips. And the DODT-filled nanopipettes are immersed in aqueous solution of TOAB (100 times dilution of the saturated solvent at 25 $^{\circ}$ C) for 5 min in order to modify the surface of the glass with positive charges. Lastly, the tips of the TOAB treated nanopipettes are then immersed in the solution with AuNPs (~ 2.21 nM) for 24 h. DODT inside the nanopipette cross-links with AuNPs and forms swab-like assembly at the glass tip. The shape of the formed *hydro*-GPS is checked under the optical microscopes, showing a typical diameter of 5 μ m. Figure S2b shows that no AuNPs could be assembled on the glass nanopipette without TOAB modification.

In order to measure the temperature change in the metallic nanopores, MOPI is used as a temperature-sensitive SERS tag². The modification steps are as follows: The *hydro*-GPS is first immersed in a methanol solution of MOPI (10 mM) for 2 h, then in 100 % methanol for 5 min. The modified *hydro*-GPS is then dried in air before use.

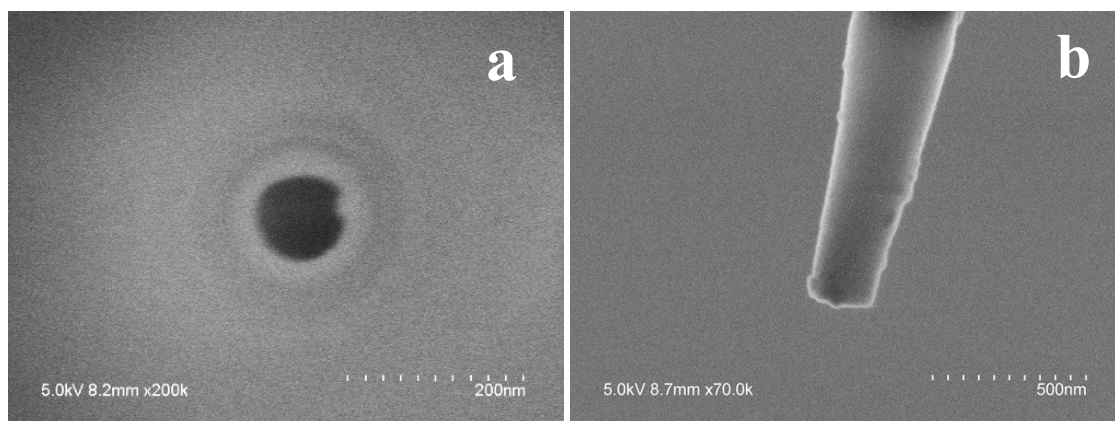


Figure S2. SEM images of the glass nanopipette with tip orifice of ~ 100 nm. (a) The top view of an unmodified glass nanopipette. (b) The side view of a glass nanopipette treated with AuNPs but without TOAB modification. The glass are pulled on a CO₂-laser-based pipette puller (P-2000, USA) with two-line program containing the following parameters: HEAT = 300, FIL = 4, VEL = 28, Del = 230, PULL = Null. HEAT = 290, FIL = 3, VEL = 25, DEL = 200, PUL = 170. *Note that different instruments may require slightly different values for these parameters to obtain equivalent nanopipettes.*

S5. The internal structure of the *hydro*-GPS

The internal structure of the *hydro*-GPS is observed by etching the spherical *hydro*-GPS using focused ion beam (FIB). The FIB instrument used Gallium (Ga) as the ion source, with a radius of about 7 nm. A layer of gold (~90 nm) is deposited prior to FIB milling. The FIB milling is then performed at a current of 11 pA at 5 keV. The *hydro*-GPS is cut vertically to the glass nanopipette layer by layer until the glass tip appears (Figure S4a). The glass tip located at the center of the cross section shows that DODT diffuses from the orifice to all directions symmetrically. A close look at the cross section of the *hydro*-GPS (Figure S4b) gives detailed structural information. The AuNPs are closely packed and form the *hydro*-GPS without cracks. The dendritic patterns above the AuNPs are formed by fused AuNPs due to the heat produced by Ga ions during the cutting process.

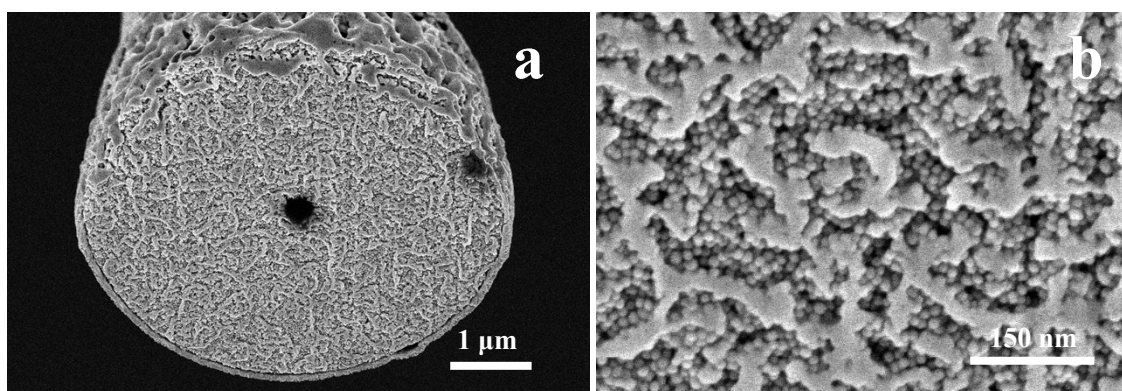


Figure S3. SEM images of *hydro*-GPS after FIB etching.

S6. Electrochemical and SERS spectroscopy measurements

A two-electrode system is used in all the measurements with one Ag/AgCl wire inserted in the glass nanopipette and another Ag/AgCl wire immersed in the bulk solution (as shown in Figure S3). The bias potential is applied auxiliary to the Ag/AgCl wire in bulk solution. In all cases, the nanopipette electrode is filled with the same electrolyte as in the bulk solution. For SERS measurement, the 633 nm radiation from a 17 mW He/Ne laser is used as the excitation source and the power at the sampling position was ~ 0.85 mW. The laser beam is focused into a spot of about $1.545\ \mu\text{m}$ with an objective lens (50 x). The SERS data are obtained *in-situ* when the *hydro*-GPS is in the testing solution with or without the applied potential. The acquisition time is usually 100 s (5 s for each scan and accumulation for 20 times). The SERS band of a silicon wafer at $520\ \text{cm}^{-1}$ is used to calibrate the spectrometer.

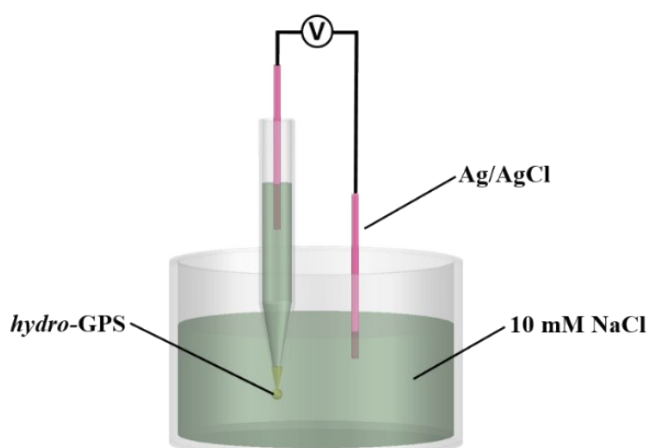


Figure S4. Schematic of the two-electrode system for electrochemical measurement.

S7. SERS activity and electrochemical properties of the *hydro*-GPS

Conventional Raman peak of the N≡C stretching in MOPI locates at 2123 cm⁻¹ (black curve in Figure S5a). Upon adsorption on AuNPs, the N≡C stretching peak shows a bit blue-shift (red curve in Figure S5a). Such blue-shift of the N≡C stretching band can be attributed to the partial donation of the lone-pair electrons of carbon in the isocyanide group to the AuNP, which increase the strength of the N≡C bond³⁻⁴.

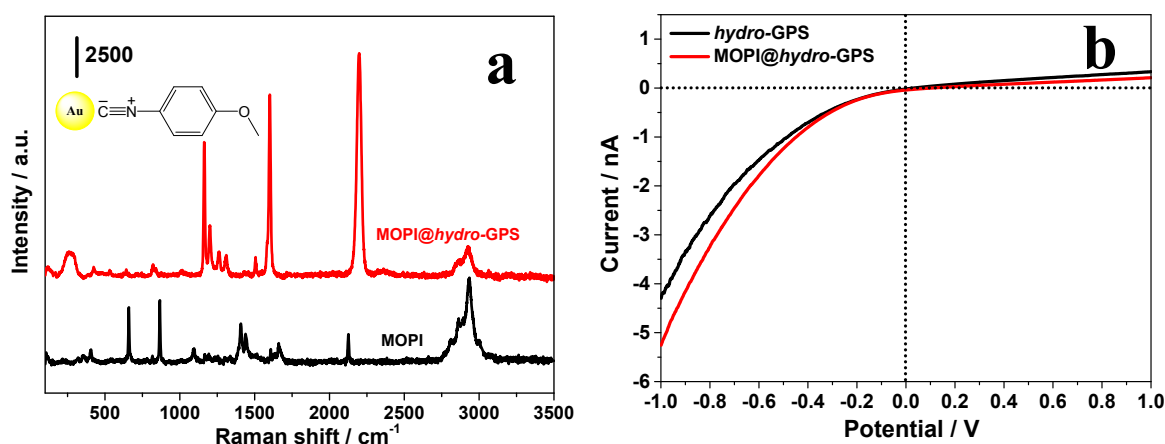


Figure S5. (a) The normal Raman spectrum of MOPI in DMF (black curve) and SERS spectrum of MOPI@*hydro*-GPS (red curve). (b) I-V curves obtained at the *hydro*-GPS and MOPI-modified *hydro*-GPS in 10 mM NaCl solution. Scan rate, 10 mV/s.

The enhancement factor (EF) is estimated according to the following equation⁵:

$$EF = \frac{I_{SERS}}{I_{bulk}} \times \frac{N_{bulk}}{N_{SERS}}$$

where I_{SERS} and I_{bulk} are the intensities of the *hydro*-GPS enhanced Raman spectrum and normal Raman spectrum of Raman reporter (MOPI), respectively. N_{bulk} is the number of reporter molecules in the bulk sample and N_{SERS} is the number of reporter molecules on *hydro*-GPS effectively excited by the laser beam, namely, the molecules within the laser beam spot. For Raman measurement of both adsorbed and bulk molecules the determination conditions are kept identical.

The Raman spectra of both 0.3643 M of MOPI dissolved in DMF and MOPI attached on the

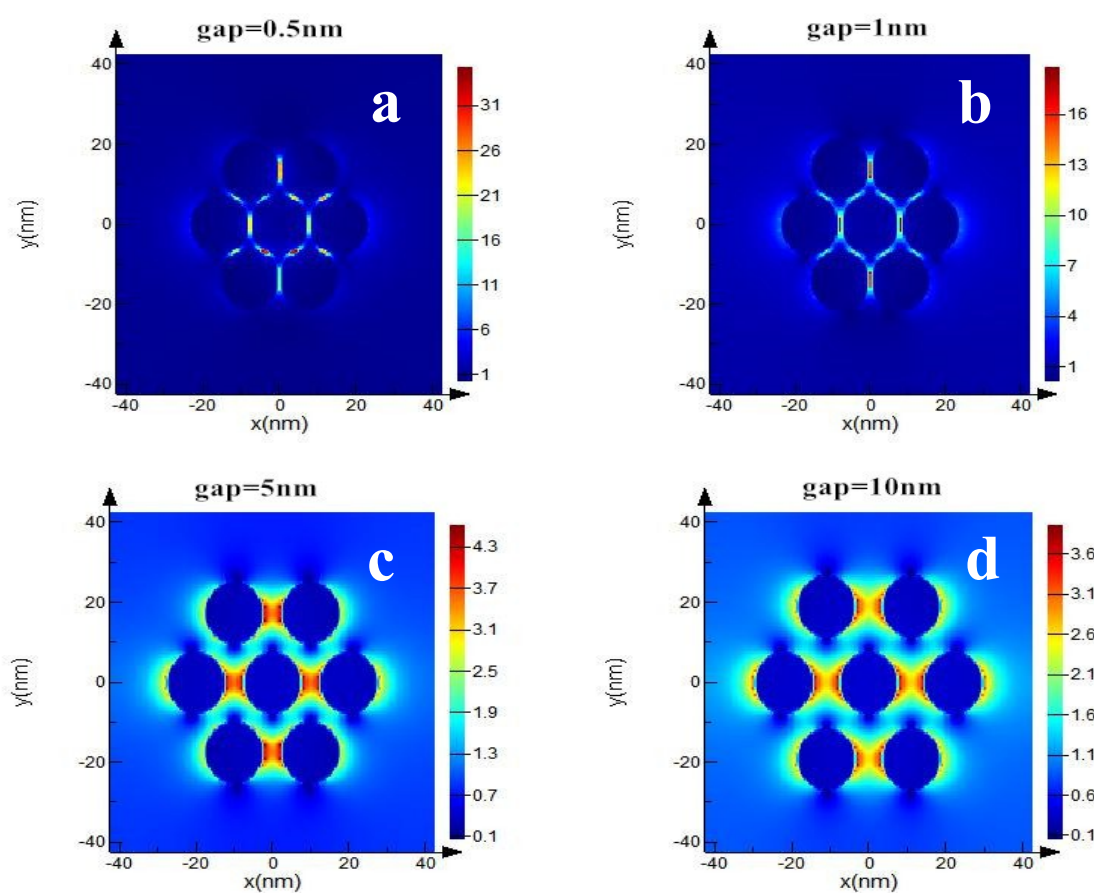
hydro-GPS are measured as shown in Figure S5a. Under the optical configuration employed in the present work, the depth of field penetration of the laser into the sample is about 3.376 μm , and the laser focus is 1.544 μm . Thus, N_{bulk} of MOPI would be 1.386×10^9 molecules. For a single monolayer formed on gold, a typical constant of 0.27 nm^2 is used⁶. N_{SERS} under the laser beam spot then is at most 9.52×10^5 molecules. Consequently, the enhancement factor is estimated to be 1.17×10^4 .

The present estimation of Raman EF is obviously underestimated because: (i) The MOPI is indeed attached on a surface already covered by dithiol, so the N_{SERS} should be much smaller than the maximum coverage of monolayer. (ii) For the small size AuNPs, only the MOPI molecules located in the gap between two AuNPs (“hot spots”) really contribute to the Raman signal. (iii) Although the skin depth of gold at 633 nm is approximately 30 nm, or 2 layers of nanoparticles in the *hydro*-GPS, the effective concentration and contribution of MOPI under the surface layer will be much less than the first layer. Therefore, though the appearance EF of *hydro*-GPS is not significantly high, we have reasons to believe that the *hydro*-GPS structure has a high Raman activity.

Figure S5b shows the ionic current rectification behavior of the *hydro*-GPS and MOPI-modified *hydro*-GPS. No obvious changes are observed showing that the modification of MOPI on *hydro*-GPS does not greatly affect the surface charge or pore size of the nanoporous structure.

S8. FDTD simulation

Since the Raman scattering enhancement scales roughly as $|E/E_0|$ (E and E_0 are the local and input fields, respectively), there is a tremendous increase of the SERS intensity for molecules adsorbed on the materials' surface beneath the particles. We make a statistics on the relationship between the field enhancement and the gap distance based on FDTD simulation (Figure S6). We assume the gap effect is the dominant factor for the field enhancement. Under our experimental conditions, the *hydro*-GPS should have a high electromagnetic field enhancement because the real gap distance is about 1-2 nm.



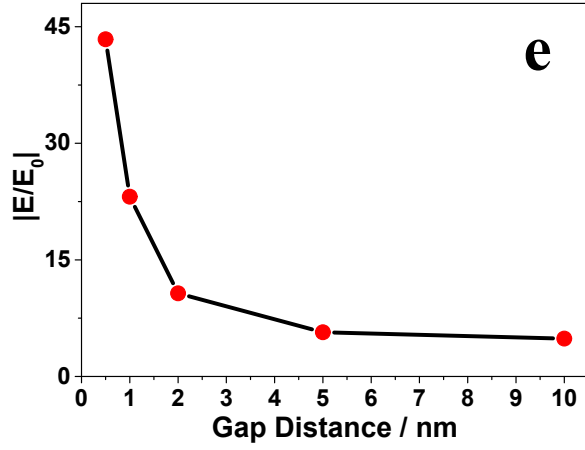


Figure S6. (a - d) FDTD calculation results of $|E|$ distributions near AuNPs dimer (diameter=15 nm) upon excitation at 633 nm with gaps of 0.5, 1, 5, and 10 nm, respectively. The excitation laser is set as a polarized light propagating along the z axis, which is perpendicular to the x-y plane. (e) The local electric field enhancement ratios against the gap of the dimer (from 0.5 nm to 10 nm).

S9. Control experiments

The effect of MOPI modification time on the Raman shift is examined to keep different experiments identical. The *hydro*-GPS is put in 0.01 M MOPI methanol and SERS spectra are measured at room temperature. With the increase of modification time, the SERS peak of $\text{N}\equiv\text{C}$ shifts to lower wave number then stabilized around 2180 cm^{-1} (Figure S7). Therefore, we chose the modification time of 2 h in order to make sure the SERS peak of the $\text{N}\equiv\text{C}$ on the *hydro*-GPS is stable enough.

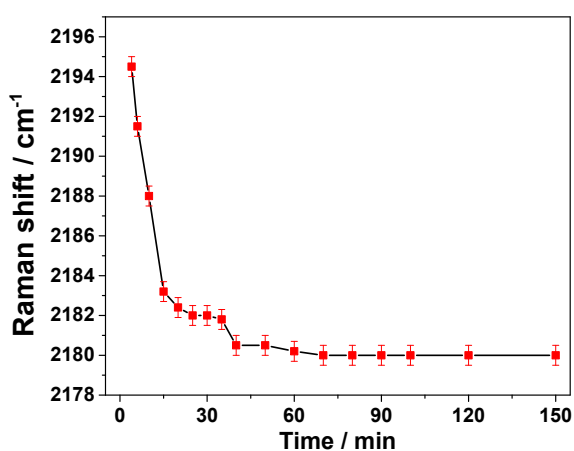


Figure S7. The dependence of $\text{N}\equiv\text{C}$ SERS peak on modification time.

The effect of ionic strength on the Raman shift is examined to keep different experiments identical. A series of solution with NaCl concentration from 0.01 mM to 1000 mM are used. The MOPI@*hydro*-GPS is put in corresponding NaCl solution and SERS spectra are measured at room temperature for different time (Figure S8). With the increase of NaCl concentration or immersion time, there are no Raman shifts in SERS spectra. Therefore, the ionic strength will not contribute to the Raman shift.

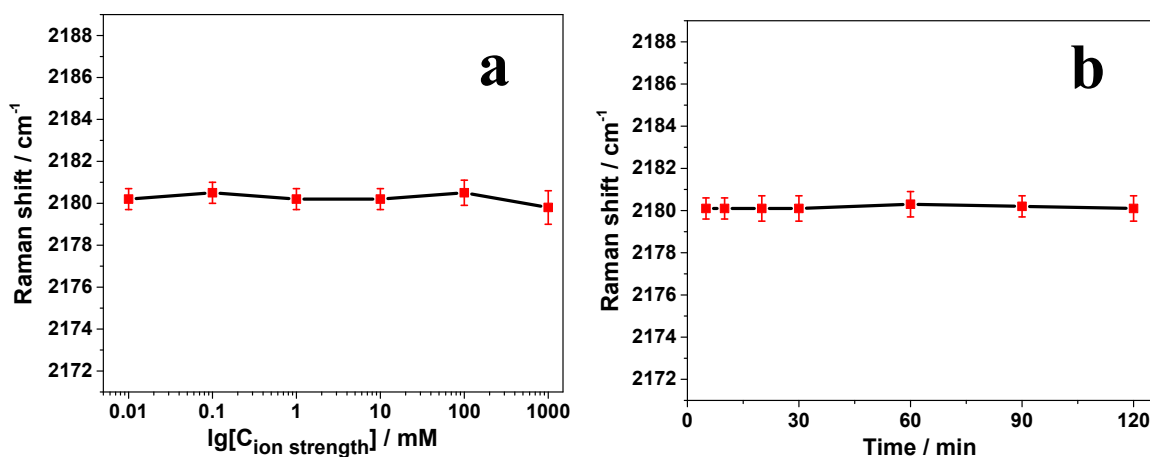


Figure S8. (a) The dependence of N≡C SERS peak on NaCl concentration. (b) The stability of N≡C SERS peak with immersion time in 10 mM NaCl.

We also examined the effect of Raman laser illuminating time on the Raman shift. The MOPI@*hydro*-GPS is put in 10 mM NaCl for 40 min with a power density of 0.85 mW under 633 nm laser and SERS spectra are measured at room temperature (Figure S9). It is found that no Raman shifts in SERS spectra after continuous illuminating for 10 min, which is much longer than the test time (100 s for each measurement). Therefore, the temperature of the MOPI@*hydro*-GPS will not change after illuminating using 633 nm laser for 100 s with a power density of 0.85 mW. Continuous illumination for 40 min results in the Raman shift to low wavenumber for about 1.9 cm^{-1} , which corresponds to a temperature increase of the whole system for about $8\text{ }^{\circ}\text{C}$. Therefore, the discontinuous SERS measurement in the present study cannot lead to substantial temperature change that may disturb the measurement of the Joule heating effect caused by ionic transport.

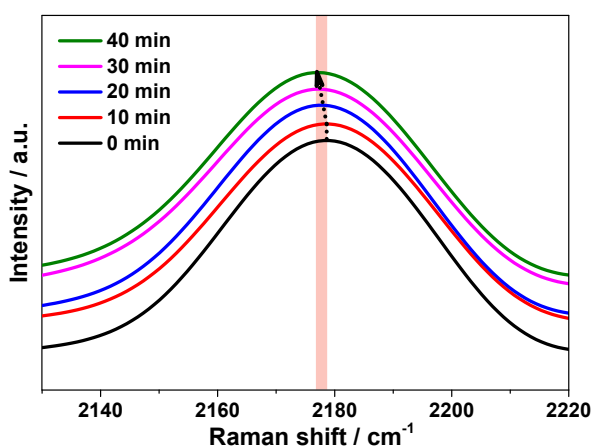


Figure S9. The dependence of N≡C SERS peak on continuous illumination using 633 nm laser with a power density of 0.85 mW.

As shown in Figure S10, when a positive potential (+5 V) is applied, the current slightly increases with an average current of 1.56 nA. The appearance of low current is not surprising because the cations in the glass nanopipette are enriched in the *hydro*-GPS, which generates an inverse potential and reduces the driving force (Figure 4a). With the bias potential changes to -5 V, the current exhibits irregular fluctuations with an average current of -2.03 nA. The fluctuation of current may be caused by two aspects: (i) the fast departure of cations from the *hydro*-GPS causes a fast increase of the current. However, the slow motion of cations from solution to the *hydro*-GPS causes the formation of a “blank” region of cation in the *hydro*-GPS. Current then drops with the increase of solution resistance. Such phenomenon is also called negative differential resistance⁷⁻⁸. (ii) The higher current induces Joule heating effect, which causes the uneven increase of temperature within the nanopores and in return enhances the fluctuation of ionic current.

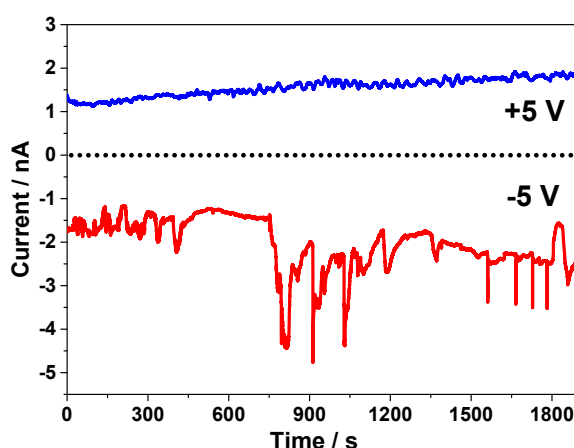


Figure S10. Time-dependent current on the *hydro*-GPS with different bias potentials.

In order to study the effect of the applied bias potential on the Raman shift we modify MOPI on an Au film electrode sputtered on a glass slide and measured a series of SERS spectra under different potentials. Ag/AgCl electrode is used as the counter electrode. SERS spectra are obtained in the potential region between 0 V and +1000 mV. As shown in Figure S11a, a noticeable blue shift of $\text{N}\equiv\text{C}$ can be observed when the surface potential is higher than +100 mV⁹⁻¹⁰. With the bias potential of +1000 mV, the SERS peak blue shifts for about 6 cm^{-1} .

In our experiments, the surface polarization potential of each AuNPs is calculated to be about 15 mV, which is much smaller than 100 mV. Therefore, the external bias potential caused polarization of the *hydro*-GPS will not contribute to the Raman shift (Figure S11b).

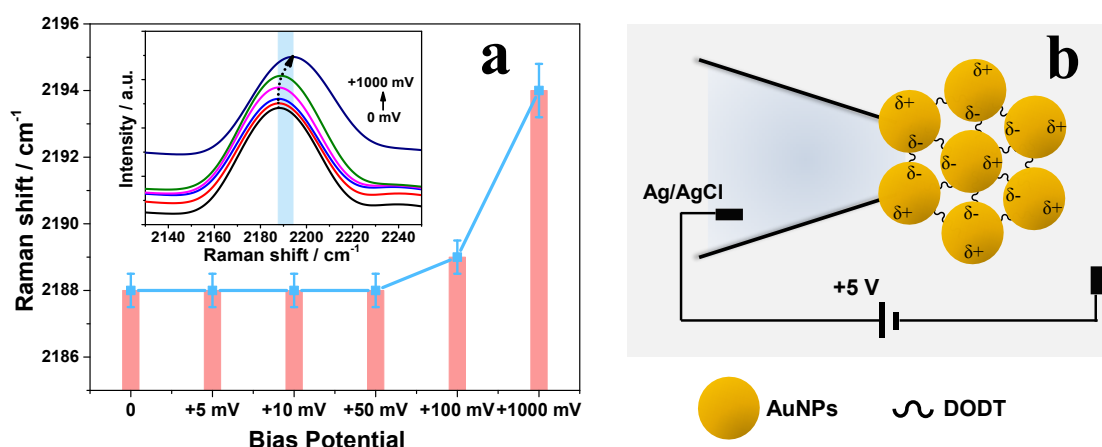


Figure S11. (a) Potential-dependent SERS peak of $\text{N}\equiv\text{C}$ on Au film immersed in 10 mM NaCl solution. Inset: corresponding SERS spectra with different applied potentials. (b) Schematic distribution of the polarization potentials on each of the AuNPs in the *hydro*-GPS.

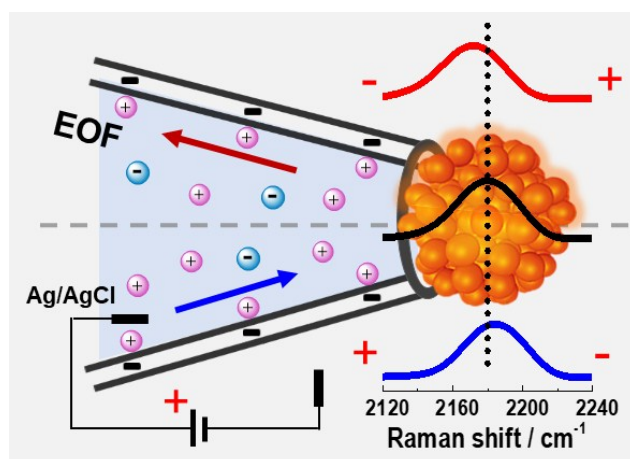


Figure S12. The schematic of ionic transport through the plasmonic nanopores with positive and negative potential.

Supplementary References

- 1 S.Zhang, J. Xia, X. Li, *Anal. Chem.*, 2008, **80**, 8382-8388.
- 2 H. Yang, L. Q. He, Y. W. Hu, X. Lu, G. R. Li, B. Liu, B. Ren, Y. Tong, P. P. Fang, *Angew. Chem. Int. Ed.*, 2015, **54**, 11462-11466.
- 3 A. C. Ontko, R. J. Angelici, *Langmuir*, 1998, **14**, 1684-1691.
- 4 S.W. Joo, Y. S. Kim, *Colloid. Surface.*, 2004, **234**, 117-122.
- 5 R. A. Álvarez-Puebla, *J. Phys. Chem. Lett.*, 2012, **3**, 857-866.
- 6 L. Stolberg, J. Lipkowski, D. E. Irish, *Electroanal. Chem.*, 1990, **296**, 171-189.
- 7 L. Luo, D. A. Holden, W. J. Lan, H. S. White, *ACS Nano*, 2012, **6**, 6507-6514.
- 8 B. K. Ridley, *Proc. Phys. Soc.* 1963, **82**, 954–966.
- 9 D. Shin, K. Kim, K. S. Shin, *Chem. Phys. Chem.*, 2010, **11**, 83-86.
- 10 K. Kim, J. W. Lee, K. S. Shin, *Spectrochim. Acta. A*, 2013, **100**, 15-20.